Atmos. Chem. Phys. Discuss., 10, 5051–5090, 2010
www.atmos-chem-phys-discuss.net/10/5051/2010/

Atmospheric Chemistry and Physics Discussions

This discussion paper is/has been under review for the journal Atmospheric Chemistry and Physics (ACP). Please refer to the corresponding final paper in ACP if available.

Transport of dust particles from the Bodélé region to the monsoon layer: AMMA case study of the 9–14 June 2006 period

S. Crumeyrolle[1,2], P. Tulet[2,3], L. Garcia-Carreras[4], C. Flamant[5], D. J. Parker[4], A. Matsuki[1,6], A. Schwarzenboeck[1], P. Formenti[7], and L. Gomes[2]

[1]Laboratoire de Météorologie Physique, Université Blaise Pascal, UMR6016, Clermont-Ferrand, France
[2]CNRM/GAME, Météo-France, URA1357, Toulouse, France
[3]LACy, Université de La Réunion, Saint-Denis, France
[4]School of Earth and Environment, University of Leeds, Leeds, UK
[5]LATMOS/IPSL, CNRS-UPMC-UVSQ, Paris, France
[6]Frontier Science Organization, Kanazawa University, Japan

[7]LISA/IPSL, Universités Paris 12 et Paris 7, CNRS, UMR 6240, Créteil, France

Received: 25 January 2010 – Accepted: 15 February 2010 – Published: 22 February 2010

Correspondence to: S. Crumeyrolle (s.crumeyrolle@opgc.univ-bpclermont.fr)

Published by Copernicus Publications on behalf of the European Geosciences Union.

Abstract

Aerosol properties were measured during an airborne campaign experiment that took place in June 2006 in West Africa within the framework of the African Monsoon Multidisciplinary Analyses (AMMA). The goal of the present study was to determine the process that facilitates the sedimentation of dust particles from the Saharan Air Layer (SAL) to the boundary layer. A significant change in the dust particle concentration measured along the meridian between Niamey (Niger) and Cotonou (Benin) was found in the boundary layer (~700 m), where the dust particle concentration increased in a zone where local emission is not possible. Moreover, the boundary layer top observed with the dropsondes launched with the F-F20 shows a strong relationship with the surface cover anomalies, with higher Boundary Layer (BL) tops over the warmer surfaces, such as croplands, as opposed to adjacent forest. A mesoscale atmospheric model with a new on-line dust parameterization, resulting from the Alfaro and Gomes (2001) parametrisation and AMMA observations, was used to interpret the impact of vegetation anomalies on dust particle sedimentation. The results of the simulation are consistent with the observations, with higher dust over the warm surface cover anomalies.

1 Introduction

Mineral dust represents the second largest component of primary particle emissions by mass, with an estimated global source strength of 1000 to 3000 Mt yr^{-1} (Ginoux et al., 2001; Houghton et al., 2001). Mineral dust consists of soil particles liberated by the wind at the surface and which can be raised to considerable tropospheric altitudes by the strong convective regimes that might develop over the desert. As a result, dust particles are transported by the winds to Europe, Middle Eastern regions and South America (e.g. Prodi and Fea, 1979; Levin et al.,1980; Talbot et al., 1986; Guerzoni et al., 1997; Avila et al., 1997; Prospero, 1999; Gobbi et al., 2003). These particles

ACPD

10, 5051–5090, 2010

contribute significantly to the global radiative budget through absorption and scattering of longwave and shortwave radiation (Houghton et al., 2001), and their indirect effect on cloud microphysics (Intergovernmental Panel in Climate Change, 2007; Twomey, 1977; Albrech, 1989; Sandu et al., 2008). The mineral dust particle effect depends on their physical, mineralogical and chemical properties that, in turn, depend on source area mineralogy, and processes on the particle surfaces during transport in dry or aqueous phases (Levin et al., 1996, Goudie and Middleton, 2001; Luo et al., 2003; Crumeyrolle et al., 2008).

Over West Africa, dust emission events occur regularly over the Tibesti and Ennedi mountains in Chad, and over the Bodélé depression due to an enhanced low-level jet feature (Washington and Todd, 2005; Washington et al., 2006; Warren et al., 2007; Todd et al., 2008b). After being transported within the Harmattan flux, which comprises the northeasterly trade winds, dust particles are observed in the Saharan Air Layer (SAL, Karyampudi et al., 1999; Parker et al., 2005a; Cuesta et al., 2009; Flamant et al., 2009b). Because of the potential of air-suspended particles for long range transport and the way these particles interact with solar and terrestrial radiation, the sedimentation process of dust particles could impact on the atmospheric stratification and thereby may modify the West African weather, and is of a major interest.

The goal of the present study is to better understand the mesoscale process that affects the dust sedimentation during its transport and to quantify the fraction of dust that is sedimented in the boundary layer during a major springtime dust event from the Bodélé and Sudan regions (Flamant et al., 2009a) in the framework of the African Monsoon Multidisciplinary Analysis (AMMA, Redelsperger et al., 2006). A detailed description of the project is available at http://www.amma-international.org/rubrique.php3?id_rubrique=1. For this purpose, airborne measurements were conducted in June 2006 along the meridian between Niamey (Niger) and Cotonou (Benin).

This paper describes the measurements of particle concentrations, optical properties and dynamical features observed during this period. Additionally, a mesoscale model with on-line dust parameterization was used to interpret the impact of the vegetation

ACPD
10, 5051–5090, 2010

anomalies on the dust particle sedimentation process. The airborne sampling strategy is described in Sect. 2. The Meso-NH mesoscale model using an explicit representation of aerosol processes is presented in Sect. 3. Section 4 outlines the observations combined with the simulation results.

2 Instrumentation

The measurements were performed during the Special Observation Period #1a (SOP1a) of the AMMA experiment on the french aircrafts (ATR-42 and F-Falcon 20) operated by the Service des Avions Français Instruments pour la Recherche en Environnement (SAFIRE). For details of the overall SOP instrumentation and its coordination, refer to Lebel et al. (2010). These aircraft were based at Niamey airport in Niger for the duration of the AMMA SOPs (Reeves et al., 2010) and performed two combined research flights during June 2006. These two combined flight patterns were conducted on 13 and 14 June 2006 along a meridian between Niamey (Niger) and Cotonou (Benin), located 750 km south of Niamey.

These flights occurred during the early afternoon when the convective mixed layer was growing relatively slowly, and the flight plans (Fig. 1) were similar. Along the meridian, the ATR-42 flew at one constant altitude (700 m a.m.s.l.) in the Boundary Layer (BL) while the French Falcon 20 (F-F20) flew in the free troposphere above the Saharan Air Layer (8000 m a.m.s.l.). Only one sounding was performed with the ATR-42 (14 June 2006), providing a rapid characterization of the inversion level and of the vertical profile of the thermodynamic and microphysical parameters, at the end of the flight. Twelve and one dropsondes were released from the Falcon-20 on 13 and 14 June, respectively (Flamant et al., 2009a).

On the ATR-42, two aerosol inlets were installed: the French Community Aerosol Inlet (CAI) and AVIRAD. The CAI is an isokinetic and isoaxial inlet with a 50% sampling efficiency estimated at 2.5 µm on which an aerosol instrumentation set was connected (Crumeyrolle et al., 2008). Two condensation particle counters (CPC TSI model 3025

ACPD
10, 5051–5090, 2010

and 3010, respectively) were used to measure total ambient aerosol concentrations (CN), a scanning mobility particle sizer (SMPS) was used to measure the number distribution of aerosol particles with diameters from 0.02 to 0.3 µm and an optical particle sizer (OPS, GRIMM model 1.108) provided particle size distributions ranging from 0.3 to 2 µm equivalent optical diameter. Data collected are used to provide the number and mass concentration. AVIRAD is an isokinetic inlet with a 50% sampling efficiency estimated at 9 µm (Filippi, 2000; Formenti et al., 2010). AVIRAD is connected to two parallel sampling lines for bulk filtration, two parallel sampling lines for 4-stage Dekati impactors, a three-wavelength (450, 550, 700 nm) nephelometer (model 3596, TSI Inc.), a seven-wavelength aethalometer (model AE31, Magee Sci.), and an optical particle sizer (OPS, GRIMM model 1.108) providing particle size distribution ranging from 0.3 to 17 µm optical equivalent diameter. The ATR-42 was also equipped for the measurements of wind, turbulent fluxes, and atmospheric state parameters.

3 Mesoscale modelling

3.1 Description

The mesoscale non-hydrostatic atmospheric model MesoNH was used in this study to complement the observations. This model has been jointly developed by CNRM (Meteo France) and Laboratoire d'Aérologie (CNRS) (Lafore et al., 1998). MesoNH simulates atmospheric conditions in the small scale (Large-Eddy Simulation type, horizontal resolution of a few metres) and synoptic scale (horizontal resolution of several tens of kilometres) and can be run in a two-way nested mode involving up to 8 nesting stages. Different sets of parameterizations have been introduced for convection (Bechtold et al., 2001), cloud microphysics (Pinty and Jabouille, 1998; Cohard and Pinty, 2000), turbulence (Bougeault and Lacarrere, 1989), biosphere-atmosphere thermodynamic exchanges (ISBA) (Noilhan and Mahouf, 1996), urban-atmosphere interactions (Masson, 2000), lightning processes (Barthe et al., 2005), gaseous chemistry (Suhre

et al., 1998; Tulet et al., 2003) and aerosol chemistry (Tulet et al., 2005).

The simulation begins at 00:00 UTC on 8 June 2006, and ends at 00:00 UTC on 14 June 2006. Two two-way nested grid domains were used. The large domain (36 km resolution) between 3.1° S and 31.7° N in latitude and 25.64° W and 35.64° E in longitude, gives a large scale synoptic view of west Africa. The embedded domain (5 km resolution) is centred over Benin and the eastern part of Niger (latitudes 4.9° N and 16.8° N and longitudes 2.2° W and 5.36° E) and gives a fine-scale view of the meridian between Niamey and Cotonou. The vertical resolution is composed of 60 stretched vertical levels reaching the altitude of 34 km; 30 levels are located in the boundary layer between the surface and 2000 m. Initialization and lateral boundary conditions of the large domain were taken from the ECMWF analysis. Vegetation types came from the ECOCLIMAP data base (Masson et al., 2003). The resolution of the ECOCLIMAP climatology is of 1 km.

3.2 Parameterization of dust size distribution

The modelling of the size distribution of mineral dust at the emission is generally treated using the Alfaro and Gomes (2001) dust parameterization (AG01), in which the dust mass size spectrum is represented by three lognormal modes with diameters centred on 1.5, 6.7 and 14.2 µm (Fig. 2). The corresponding mass fractions are about 1%, 36% and 63%. The corresponding median diameters for the number size distribution are 0.64, 3.45, and 8.67, respectively, with 74% of the number concentration in the finer mode centred at 0.64 µm (Fig. 2). During the June SOP, a number size distribution was measured onboard the ATR-42 during flight 21, while the aircraft was flying very close above the ground near a source area. This measurement confirms the existence of a particle mode centred around 0.64 µm but indicates that almost 99% of the number concentration is included in two other particle modes finer than that centred around 0.64 µm (Fig. 2b). Even if the AG01 parameterization represents the mass fluxes of emitted particles well, it seems to largely underestimate the number concentrations of fine particles.

To improve the dust size spectrum parameterisation (Todd et al., 2008a), we propose to build a new spectrum composed of three modes based on the AG01 scheme and the AMMA observations. The particle mode of the number distribution centred on 0.64 µm, which is common to AMMA observations and AG01 scheme, is used as the reference particle mode.

The new dust size spectrum is constrained in order to have the same total number concentration as the observed number size distribution and the same total volume concentration as the AG01 scheme. Thus, to represent the mass size distribution of this new scheme, we introduce a larger mode (Dp=11.6 µm) derived from a combination of larger particle modes of AG01 by respecting the sum of their volume fraction (99%). Then, to best represent the number concentration, we introduce a fine mode (Dp=0.2 µm) derived from a combination of finer particle modes observed during the AMMA flight 21 and respecting the total number concentration observed (1430 cm^{-3}). Finally, the dust number and mass size spectra are represented by three lognormal modes (Fig. 2). The lognormal parameters of the deduced size distribution which will be used in MesoNH are given in Table 1. With this new size distribution (NSD), the number concentrations, made of more than 97% of fine particles, are considerably improved. As a result, the impact of very small particles on the radiative budget and their feedback on the West African weather should be appreciably better represented. Furthermore, the aerosol budget may be compared to the observations and fixed with three variables: the aerosol optical depth (AOD), the mass concentration and the number concentration.

Mineral dust emissions and transport are parameterized by Grini et al. (2006). Regarding emission processes, dust aerosols are mobilized using the Dust Entrainment and Deposition model (DEAD) (Zender et al., 2003) which calculates dust fluxes from wind friction speeds. The physical basis of the model is taken from Marticorena and Bergametti (1995) where dust fluxes are calculated as a function of saltation and sandblasting processes. Here, the emission of dust aerosols is calculated directly from Interactions between the Soil Biosphere and Atmosphere (ISBA) surface parameters,

and then sent to the atmosphere consistent with the fluxes of momentum, energy and humidity. In this parameterization, the three dust aerosol populations, proposed in this study, are transported by the ORILAM lognormal aerosol scheme (Tulet et al., 2005).

To interpret the observational results, four different simulations have been performed by using the mesoscale non hydrostatic atmospheric model MesoNH. First, to highlight sedimentation processes, two different simulations have been realized, one which takes into account the dust sedimentation (SED) and the other one which does not (NOSED). The comparison of the results is only possible if the atmospheric dynamics are consistent between the two simulations. As dust particles have a large impact on the radiative budget and thus on the atmospheric dynamics, both absorption and, most importantly, diffusion of dust particles have to be turned off in both simulations. However, in reality dynamical features may have a feedback on the stratification of the dust particles in the atmosphere. Then, for each simulation (SED and NOSED), two versions have been carried out: one where the radiative impact of dust has been taken into account (RAD) and another one without this radiative impact. In the following parts, the dynamical features will be discussed using the simulation RAD-SED and the processes leading to sedimentation will be explored using the NORAD-SED and NORAD-NOSED simulations.

3.3 Comparison of observed and simulated parameters

3.3.1 Aerosol distribution

During the period from 9 to 14 June 2006, satellite data indicate that numerous dust sources were active (Flamant et al., 2009a). Figure 3 represents the simulated aerosol optical depth over West Africa during the main dust outbreaks of June. During the AMMA campaign, AERONET photometers were located at Maine Soroa (Niger, 12.02° E/13.28° N), Banizoumbou (Niger, 2.66° E/13.54° N) and Djougou (Benin, 1.6° E/9.76° N). On Fig. 3, the observed AOD (560 nm) is shown in the small boxes to be compared to the simulation (Fig. 3). The Maine-Soroa station is located in the Sahelian

ACPD
10, 5051–5090, 2010

region downwind of the lake Chad source area while the two other AERONET stations are located close to big cities (Niamey 13.5° N/2.2° E, Parakou 9.2° N/2.61° E).

On the 9 June, ECMWF data highlights nocturnal jets (Flamant et al., 2009a) strong enough to lift soil particles by saltation and generate high dust concentration at the surface as simulated by the model (Fig. 3a). Indeed, over the two major sources the AOD is on average about 4. Over the rest of West Africa the AOD is almost zero. The observed AOD at Maine Soroa (2.7) is well represented by the model while the simulated AOD at Banizoumbou (AOD_{obs}=1.1) and Djougou (AOD_{obs}=0.64) are largely underestimated. This underestimation is probably due to pollution and dust particles generated previously which are not taken into account in the simulation. During the following days, the generated particles are progressively advected westward to the Atlantic Ocean between 9 and 14 June and the observed AOD reaches higher values well represented by the model, for example, 2.5 and 1 respectively at Banizoumbou and Djougou on the 10 June (Fig. 3b). Until the 12 June, the simulated low level winds remain important over the source regions and thus AOD values exceeding 3 have been simulated (Fig. 3a, b, c, d). On the 14 June, the transported dust particle concentration is almost homogeneous over the whole of West Africa and the AOD is on average about 1 (Fig. 3f).

During the period of interest (9–14 June), several Mesoscale Convective Systems (MCS) were triggered over West Africa. The MCS-tracking (Mathon et al., 2002) and the Radagast products (Miller and Slingo, 2007) allowed us to watch the MCS formation and to follow its trajectory along West Africa (data available at the AMMA Operational Center, http://aoc.amma-international.org/) and to have a dust diagnostic derived from three of the SEVIRI infrared channels (data available http://radagast.nerc-essc.ac.uk/Data.htm) respectively. On 11 June, one massive MCS, initiated over Togo (west of Benin), propagates along the coastline to the Atlantic Ocean. The gust front induced by this MCS and situated in front of the MCS does not involve dust emission at the rear of the MCS (Crumeyrolle et al., 2008), over Benin. On 12 and 13 June, small convective cells appear (over Ilorin and 2° N of Djougou) but do not generate dust particles at the

surface of the continent. Thus, dust particles observed on Fig. 3 over the meridian from Niamey to Cotonou are only a consequence of long range transport from dust sources (Bodélé and Sudan).

The Bodélé and the Sudan are the most important sources of dust particles for this event but the western part of Algeria is also highlighted as a source of dust particles. Indeed, the maximum AOD value is about 2 indicating that the dust concentration lifted up in this zone is weaker than over the main source regions, but not negligible. For comparison, during the intense dust outbreak of 7–13 March 2006, the AOD reached 3.8 and 3.5 at Ilorin (Nigeria) and Banizoumbou, respectively (Tulet et al., 2008).

The aerosol number concentrations measured onboard the ATR-42 with the SMPS and the OPS as a function of altitude during a vertical sounding on 14 June between 15:15 UTC and 15:30 UTC (Fig. 4a) were converted to mass concentrations (Fig. 4b) using a density of 2.5 g cm^{-3} in order to give the mean profile of aerosol mass concentration for the zone considered (i.e. 2° E/12.6° N close to Banizoumbou). These data are compared to the vertical profile of dust number and mass concentration simulated over Banizoumbou on 14 June. The spatial variability (1° around the ATR-42 sounding area) of the simulated data is represented by the blue area. A size cutoff of 2.5 µm similar to the 50% sampling efficiency of the aerosol inlet was applied to the calculation in order to compare simulated aerosol profiles to airborne observations for particles with diameter lower than 2.5 µm. The Carbon Monoxide (CO) concentration is used as a tracer to highlight polluted air masses (Fig. 4c, red line). The Angström coefficient (Fig. 4d, black line) is calculated using the scattering coefficients at two wavelengths (450 and 700 nm, Fig. 4d) and depicts the wavelength dependence of the scattering coefficients. Low values of the Angström coefficient highlight low wavelength dependence associated with large particles, i.e. dust particles.

In the boundary layer, between the surface and 1200 m (Fig. 4b), the observations highlight a well-mixed layer with a steady mass concentration of 20 µg m^{-3}. The particle number concentration profile is slightly different and shows a decrease as a function of altitude. Indeed, the number concentration of particles is about 4000 cm^{-3} at the

ACPD
10, 5051–5090, 2010

surface and about 3150 cm^{-3} at the top of the boundary layer. Furthermore, the simulated dust number and mass concentrations are constant and clearly underestimated in the boundary layer (100 cm^{-3} and 8 $\mu g\, m^{-3}$). This underestimation can be attributed to the simulation's restriction to one type of particle; i.e. dust particles. Actually, the average concentration of CO is significant, about 180 ppb, and similar to mean values (200 ppb) found previously over savannah fires (Cofer et al., 1996). This high CO concentration suggests that a large amount of aerosol particles from local pollution or from biomass burning events are also sampled by the ATR-42. The calculated Angström coefficient value (0.35 in average) indicates a mixture of dust and pollution.

The SAL, between 1200 and 3100 m (Fig. 4b), is characterized by a maximum in the mass particle concentration (32 $\mu g\, m^{-3}$) consistent with a previous study (Karyampudi et al., 1999). Moreover, one can note the high concentration and variability of CO (100–180 ppb) in this layer. Between 1200 and 2300 m, the CO concentration slightly decreases with altitude, down to 100 ppb, which corresponds to the background concentration of CO in the upper layer and in the Northern Hemisphere (Colomb et al., 2006). As the SAL is decoupled from the surface below and is more closely linked to the desert regions, the CO concentration and the Angström coefficient highlight that the SAL is subject to strong exchanges with the boundary layer (Parker et al., 2005b). These strong exchanges lead to the presence of different types of particles in the SAL and thus an underestimation of the particle number (66% on average) concentrations in the simulation. Between 2500 and 3100 m, one can see an increase in the particle number concentrations in the profile (~1000 cm^{-3}) associated with an increase in the CO concentration which reaches 140 ppb. This particular shape is a consequence of long range transport of biomass burning from Central and South Africa. Indeed, the MOPITT data show a plume of CO coming from the south of West Africa (http://www.acd.ucar.edu/mopitt/MOPITT/data/plots/maps.html). Thus, in this specific range of altitudes, the simulated concentration is, once again, underestimated (630 cm^{-3}).

Above the SAL is the free troposphere wherein the particle and CO concentrations are, on average, weak (390 cm^{-3}, 8 $\mu g\,m^{-3}$ and 100 ppb). In this layer, the Angström coefficient values are always lower than 0.2 and the main particle type sampled with the ATR-42 is dust. Thus, the number and mass concentrations are well represented in the simulation (300 cm^{-3}, 4 $\mu g\,m^{-3}$). Note that while the 14 June profile described in this section was strongly influenced by biomass burning and local pollution, the meridional profile of 13 June was dominated by mineral dust: this earlier flight will be described in the next section.

3.3.2 Dynamical features

Figure 5 shows the vertical cross section, along the ATR-42 flight track of the meridional component of the wind velocity ($m\,s^{-1}$) simulated by Meso-NH (RAD-SED simulation) at 12:00 UTC on 13 June 2006. This vertical cross section highlights specific dynamical features that occur over West Africa. In the lower layer of the atmosphere (<1500 m), the meridional wind speed is positive between 6.5 and 13.2° N and becomes negative further to the north which depicts the monsoon flux and the Harmattan flux respectively. The monsoon flux is deeper (1500 m) and stronger (>5 $m\,s^{-1}$) in the southern part than in the northern part of West Africa as shown previously by Parker et al. (2005). Above 1500 m and close to the Inter Tropical Discontinuity (ITD), located at 13.2° N, the Harmattan flux overrides the monsoon flux and reaches the maximum negative wind speed (< −5 $m\,s^{-1}$).

The F-F20 flew, in coordination with the ATR-42, between 1.5° E/15° N and 1.5° E/4° N at 8000 m a.m.s.l. on the 13 June 2006 (Flamant et al., 2009a). The vertical distribution of atmospheric dynamic and thermodynamic parameters were provided by dropsonde measurements along the meridional transect. Figure 6 shows the evolution of vapour mixing ratio ($g\,kg^{-1}$), wind speed ($m\,s^{-1}$) wind direction (°N) and potential temperature (K) observed by four dropsondes (DS), whose location is shown in Fig. 5, and simulated by MesoNH. The wind direction and the vapour mixing ratio (RV) profiles depict the dynamical situation shown in Fig. 5, i.e. the Monsoon Layer, with the

Harmattan Layer above it. Indeed, between 1000 and 1500 m altitude, the meridional wind direction changes abruptly from south-westerly (Fig. 6a, b) and southerly (Fig. 6c, d) to easterly and north-easterly respectively. In the same altitude range, the vapour mixing ratio profile is strongly decreasing which indicates the passage from a humid layer to a dry layer. These key dynamical and thermodynamic parameters are well represented in the simulation, although at 10° N (Fig. 6b) the top of the monsoon layer is overestimated by 400 m. The observed and simulated wind speed profiles are similar; nevertheless the simulated values are most often underestimated in the monsoon layer (2–4 m s^{-1}) as well as in the Harmattan layer (2 m s^{-1}). The simulated and observed potential temperature profiles are almost the same for the four dropsondes.

The above results show that the aerosol particle depth and concentrations as well as the key dynamical and thermodynamic parameters are well represented in the simulation. Thus, the simulation results will be used in the next part to complement and interpret the observations.

4 Results

The concentration of particles with diameter higher than 0.5 µm ($CN_{Dp>0.5\mu m}$) and the aerosol scattering coefficients were first used to characterize the evolution of the particle properties (optical properties, concentration) along the meridional flight plan (Fig. 7). Then, the temperature gradient, the potential temperature, the surface temperature, the meridional wind velocity and the percent of forest/shrub cover were used to find out the link between the surface cover and the dynamics in the boundary layer (Fig. 8). Afterwards, the simulation results were analysed in the same manner.

4.1 Observations of sedimentation and entrainment processes

Figure 7a shows the evolution of the total concentration of particles with diameter higher than 0.5 µm ($CN_{Dp>0.5\mu m}$) and of the aerosol scattering coefficients measured

ACPD
10, 5051–5090, 2010

as a function of latitude during the flight from Niamey (13.51° N) to Cotonou (6.36° N) between 10:30 UTC and 13:30 UTC on 13 June while Fig. 7b shows the evolution of the Angström coefficient. The tendencies of the $CN_{Dp>0.5\mu m}$ concentration and the aerosol scattering coefficients are similar during the whole flight. At the beginning of the flight (North), the dust concentration is high and reaches 16 cm^{-3} at 12.6° N. Scattering coefficients at all wavelengths are higher than 85 Mm^{-1} and the calculated Angström coefficient is low (0.2). Thus, because of the little wavelength dependence of the scattering coefficient, the majority of particles composing $CN_{Dp>0.5\mu m}$ are identified as dust particles.

Moving southward, the $CN_{Dp>0.5\mu m}$ concentration decreases up to a first minimum (6.5 cm^{-3}) at 11.5° N. In this area the surface cover is sufficient to inhibit the local production of dust particles (Flamant et al., 2007, 2009a) which seems to be consistent with the decrease of $CN_{Dp>0.5\mu m}$ concentration. At 10.8° N, the $CN_{Dp>0.5\mu m}$ concentration reaches a second maximum (17 cm^{-3}) associated with a second maximum of scattering coefficient (90 Mm^{-1}) at all wavelengths. This peak of $CN_{Dp>0.5\mu m}$ is also associated with an increase of the Angstrom coefficient (up to ~0.3). Nonetheless, in this area the vegetation cover (0.2, Fig. 8) is still too important to allow local dust production. Indeed, the maximum value of the $CN_{Dp>0.5\mu m}$ concentrations measured at the super-site of Djougou during the period of interest is about 3 cm^{-3} on 14 June. As the ATR-42 flew at a constant altitude (700 m) which was located in the middle of the monsoon layer, the measurements were never sampled in the SAL and Fig. 7 shows only the evolution of dust concentrations in the monsoon layer. These measurements confirm that dust particles observed with the ATR-42 are not generated at the surface but their presence in this zone is only due to long range transport from the northern region. South of 10° N, the $CN_{Dp>0.5\mu m}$ concentration as well as the scattering coefficients decrease with latitude. Moreover, the wavelength dependence of the scattering coefficient (represented by the Angstrom coefficient) becomes more important as the latitude decreases. Thus, between 6° N and 10° N, particles from polluted or

ACPD
10, 5051–5090, 2010

biomass-burning zones are dominant. One can note higher values of the $CN_{Dp>0.5\mu m}$ concentration and the scattering coefficient at 6.8° N and 8.9° N due to polluted plumes originating from urban centers (Cotonou and Parakou).

Recent studies investigated the impact of vegetation heterogeneities on the dynamics within the planetary boundary layer (Taylor et al., 2003, 2007; Garcia-Carreras et al., 2010). These studies highlighted a strong relationship between the boundary layer temperatures, the boundary layer top, the meridional wind velocity and the fraction of forest or shrub cover. The boundary layer temperature anomalies caused by variations in sensible heat flux or Bowen ratio at boundaries between forest/shrub and cropland lead to an increase in the boundary layer top. The vertical distribution of dynamic and thermodynamic quantities, which were used to estimate the BL height, were documented using dropsonde measurements. As the ATR-42 flew before the F-F20, the boundary layer height can therefore be expected to have increased during the delay between both aircraft due to the surface heat fluxes and the resultant entrainment of residual-layer air. Thus, the BL height has been estimated using the method described in Hopkins et al. (2009). Figure 8 shows the calculated boundary layer height and the amount of forest/shrub cover derived from the GlobCover Land Cover map as in Garcia-Carreras et al. (2010) along the meridian from Niamey to Cotonou. The BL height increases suddenly at 6.3° N, corresponding to the passage over the coastline, and slightly increases from 950 m (6.6° N) to 1250 m (9.9° N). In the same latitude range, the forest/shrub cover increases abruptly at 7.1° N (>50%) and then becomes stable (35%). Over the area running from 9.9° N to 12.3° N, the forest/shrub cover diminishes (15%) from 9.9° N to 11.1° N, and as a consequence of an increase in Bowen ratio, the surface temperature increases. Thus, the BL height reaches maximum values (1500 m). These results show a strong relationship between surface cover and the height of the boundary layer (as inferred from BL temperature), consistent with the results of Garcia-Carreras et al. (2010) from flights later in the season. This coupling between the surface and the boundary layer dynamics occurs exactly in the same area of high dust content.

ACPD
10, 5051–5090, 2010

Garcia-Carreras et al. (2010) show that the vegetation anomalies are related to the vertical transport of isoprene from the surface to the upper layers, thus, amplifying exchanges between the monsoon flux (high content of isoprene/low content of dust particles) and the Harmattan layer (low content of isoprene/high content of dust particles). In this case, the growth of the BL leads to entrainment of dusty air from the upper layer (SAL) into the BL. Thus, the vegetation anomalies are associated to the presence of high concentrations of dust particles in the monsoon flux. To complement the observations and interpret the results, a simulation exercise was carried out.

4.2 Numerical modelling: sedimentation and entrainment quantification

Two separate simulations have been done, one which takes into account the dust sedimentation (SED) and another one which does not take into account the dust sedimentation (NOSED). In the following part, the dust radiative impact has been turned off, in order to have similar atmospheric dynamics in both simulations (NORAD). Thus, the only variable differing between both simulations is the dust sedimentation. The vertical cross-section of dust number concentration of the SED simulation is given in Fig. 9. The northern part of the domain, which corresponds to an arid region of sparse vegetation, is subjected to strong low level winds at the surface and numerous dust particles (3000 cm^{-3}) are produced in this region. These freshly generated particles are then transported in a southwestward direction within the Harmattan flux over the monsoon flux. Both layers, the monsoon flux and the SAL, are clearly distinguished using the dust concentration gradient. Indeed, the dust particle concentration is lower than 500 cm^{-3} in the monsoon layer (excluding the ITD region (13.2° N) where dust particles are carried away by turbulence in the monsoon flux Bou Karam et al., 2008) and on average about 1500 cm^{-3} in the SAL.

Figure 10 shows the evolution of the dust mass size distribution as a function of latitude for both simulations SED and NOSED (line and dashed line, respectively). For the NOSED simulation, the amplitude for the coarse mode decreases with latitude due to diffusion of dust particles during their transport, while for the SED simulation the

evolution of size distributions shows a decrease of the amplitude of the coarse mode up to 10° N and then an increase due to the sedimentation process of dust particles from upper layers. The comparison of dust particle size distributions of both simulations (SED/NOSED) gives the quantity of sedimented dust for each mode and at each latitude. At 12° N, about 50% of the mass of larger dust particle has sedimented while the sedimentation process leads to an increase of only 2% of the mass of particles forming the medium mode of Table 1. By the time air reaches the southern part of the section, at 6° N, more than 85% of particles of the coarse mode and about 10% of those of the medium mode have sedimented. In terms of particle number concentrations, this sedimentation process leads to a gain of about 100 particles, corresponding to 3600 g m^{-3} at 2000 m. The sedimentation process of dust particles is thus two times more efficient in the southern part of the domain than close to source regions.

In order to have a general view of the dust particle sedimentation process, the difference of dust mass concentrations between the simulation without sedimentation and the simulation including sedimentation (NOSED–SED) is given in Fig. 11. Negative mass concentrations correspond to sedimented particles and positive concentrations correspond to dust particles that are removed because of the sedimentation process. The top of the monsoon flux, marked with the black line (Fig. 11), has been delineated using the method given by Lamb (1983). Between 6° N and 9° N, the difference of dust concentration is minimum (~ -1000 cm^{-3}) in both the monsoon layer and in the Harmattan layer. These particles are mainly coming from upper layers where the difference in dust concentrations is maximum (layer at 3500 m). Furthermore, this sedimentation process leads to the presence of dust in the boundary layer down to 800 m, corresponding to the higher altitude of the ATR-42 flight plan, between 7.3° N and 8.8° N.

The comparison of Figs. 7 and 11 highlights some differences in the latitude range where the maximum dust concentration is located. To understand why there is this discrepancy between simulation results and observations, the surface cover has to be studied. As the fraction of forest/shrub cover used in the simulation is an ECOCLIMAP climatology with 1km of resolution (Fig. 12), the comparison with another climatology,

ACPD
10, 5051–5090, 2010

Globcover Land Cover map, with higher resolution (300 m, Fig. 8b) highlights some inconsistencies. Indeed, the forest/shrub cover is much more important (30%) between 6° N and 7° N in ECOCLIMAP than the Globcover surface cover and clearly weaker (20%) between 7° N and 8° N (Fig. 12). In the northern part of the domain, the ECOCLIMAP forest/shrub cover is always higher than 40% and frequently exceeds 55%. As a result, the surface cover anomalies are located in the southern part of the domain. The difference of surface cover at 10° N between observations and simulation results was previously shown in Fig. 6b. Indeed, the forest/shrub cover in the simulation is more important at 10° N than in the observations, thus the heat flux is weaker and the top of the boundary layer is lower.

Finally, the comparison between observations and the simulation results shows that the presence of vegetation anomalies and dust are closely linked. Indeed, a reduction in forest or shrub cover lead to an increase in the BL height (inferred from BL temperature in the observations, and consistent with the model results) and leads to exchanges between the monsoon layer and the Harmattan layer via entrainment. Thus, aerosol particles and compounds produced in the monsoon layer are measured in the upper layer (Garcia-Carreras et al., 2010) while aerosol particles transported from desert regions by the Harmattan flux are observed in the monsoon layer. These mechanisms imply that we should infer a significant diurnal cycle in the mechanisms of dust sedimentation from the SAL to the monsoon layer. During the day, the sedimentation is modulated by the differing rates of BL entrainment over differing surfaces. At night, when the atmospheric profile is more stable (Parker et al., 2005b), sedimentation acts alone and is likely to be independent of the underlying surface.

5 Conclusion

This paper describes the impact of vegetation anomalies on mineral dust particle sedimentation and entrainment observed during the AMMA experiment by using a combination of airborne observations and simulation exercises. Airborne measurements

of aerosol characteristics were carried out along the meridian from Niamey (Niger) to Cotonou (Benin) on 13 and 14 June 2006. The measurements were performed by two aircraft (ATR-42 and F-F20) flying on the same meridian at two different altitudes (700 m and 8000 m, respectively). Observations were then interpreted using a mesoscale model simulation in order to explain the presence of high dust content over an area where local production is largely restricted by the surface cover.

The ATR-42 observations highlight that the boundary layer temperature is linked with the surface cover, which produces a strong relationship with the dust particle concentrations in the boundary layer. Consistent with model simulations, we infer that the relationship between dust particle concentration and BL temperature occurs due to the deepening of the BL over warmer surfaces, by entrainment. Indeed, the optical particle sizer (OPS GRIMM) and the nephelometer measurements show the presence of mineral dust particles highly concentrated between 10° N–11.7° N. As local emissions are inhibited in this zone, these particles are coming from long range transport within the SAL and sedimentation and entrainment processes in the boundary layer. This zone of high dust content is slightly shifted to the North due to the general circulation over West Africa (monsoon winds).

Particle size distributions observed close to the source region (>15° N and >4.5° E) have been used to improve the dust size spectrum parameterization. This new dust parametrisation implemented in Meso-NH allows the model to best represent the number and mass distributions of dust particles. The simulation results highlight, as in the observations, an increase of the boundary layer top induced by vegetation anomalies but closer to the coastline (7° N–8° N). Indeed, the surface cover used in Meso-NH is an ECOCLIMAP climatology with a resolution of 1 km and is not the same as the GlobCover Land Cover map products (resolution 300 m). Finally, two mesoscale simulation exercises have been done to complement these results, one simulation with dust particle sedimentation (SED) and the other one without dust sedimentation (NOSED). The comparison of SED and NOSED simulation quantifies the concentration of dust particles which sediment, and the location of this process. The sedimentation process

ACPD
10, 5051–5090, 2010

leads to the vertical transport of dust particles (1000 µg m^{-3}) from the Harmattan layer (or SAL) to the monsoon layer between 6° N and 9° N. This mechanism may involve deep vertical transport (up to 800 m) of dust particles in the monsoon layer, between 7.3° N and 8.8° N. Thus, the comparison results confirm how the sedimentation and entrainment processes are linked with the mesoscale vegetation anomalies observed in the region.

Acknowledgements. This work has been supported by the African monsoon multidisciplinary analysis (AMMA) project. Based on a French initiative, AMMA was built by an international scientific group and is currently funded by a large number of agencies, especially from France, UK, USA and Africa. The authors wish to thank the SAFIRE (Service des Avions Francais Instruments pour la Recherche en Environnement) for preparing and delivering the research aircrafts (ATR-42 and Falcon-20). The authors are grateful to the MesoNH team for their assistance. Suzanne Crumeyrolle has been supported by CNRS fellowship (contract no. 167641). Luis Garcia-Carreras has been supported by NERC studentship NE/F007477/1. AMMA-UK is supported by NERC grant NE/B505538/1.

The publication of this article is financed by CNRS-INSU.

References

Alfaro, S. C. and Gomes, L.: Modeling mineral aerosol production by wind erosion: Emission intensities and aerosol size distributions in source areas, J. Geophys. Res., 106(D16), 18075–18084, 2001.

Albrecht, B. A.: Aerosols, cloud microphysics, and fractional cloudiness, Science, 245, 1227–1230, 1989.

Avila, A., Queralt-Mitjans, I., and Alarcon, M.: Mineralogical composition of African dust delivered by red rains over the northeastern Spain, J. Geophys. Res., 102, 21977–21996, 1997.
Barthe C., Molinie, G., and Pinty, J. P.: Description and first results of an explicit electrical scheme in a 3d cloud resolving model, Atmos. Res., 76(1–4), 95–113, 2005.
Bechtold, P., Bazile, E., Guichard, F., Mascart, P., and Richard, E.: A mass-flux convection scheme for regional and global models, Q. J. Roy. Meteor. Soc., 127, 869–886, 2001.
Bougeault, P. and Lacarrére, P.: Parametrization of orography-induced turbulence in a meso-beta model, Mon. Wea. Rev., 117, 1872–1890, 1989.
Bou Karam, D., Flamant, C., Tulet, P., Todd, M. C., Pelon, J., and Williams, E.: Dry cyclogenesis and dust mobilization in the Inter Tropical Discontinuity of the West African Monsoon: a case study, J. Geophys. Res., 114, D05115, doi:10.1029/2008JD010952, 2008.
Cofer III, W. R., Levine, J. S., Winstead, E. L., Cahoon, D. R., Sebacher, D. I., Pinto, J. P., and Stocks, B. J.: Source compositions of trace gases released during African savanna fires, J. Geophys. Res., 101(D19), 23597–23602, 1996.
Colomb, A., Williams, J., Crowley, J., Gros, V., Hofmann, R., Salisbury, G., Klüpfel, T., Kormann, R., Stickler, A., Forster, C., and Lelieveld, J.: Airborne Measurements of Trace Organic Species in the Upper Troposphere Over Europe: the Impact of Deep Convection, Environ. Chem., 3, 244–259, 2006.
Cohard, J. M. and Pinty, J. P.: A comprehensive two-moment warm microphysical bulk scheme, ii: 2d experiments with a non hydrostatic model, Q. J. Roy. Meteorol. Soc., 126, 1843–1859, 2000.
Crumeyrolle, S., Gomes, L., Tulet, P., Matsuki, A., Schwarzenboeck, A., and Crahan, K.: Increase of the aerosol hygroscopicity by cloud processing in a mesoscale convective system: a case study from the AMMA campaign, Atmos. Chem. Phys., 8, 6907–6924, 2008, http://www.atmos-chem-phys.net/8/6907/2008/.
Cuesta, J., Marsham, J. H., Parker, D. J., and Flamant, C.: Dynamical mechanisms controlling the vertical redistribution of dust and the thermodynamic structure of the West Saharan atmospheric boundary layer during summer, Atmos. Sci. Lett., 10, 34–42, doi:10.1002/asl.207, 2009.
Filippi, D.: Etude et développement d'un instrument aéroporté destiné à la collecte des aérosols et à la mesure du Radon 222 par son dépôt actif, thèse Univ. Paris VI, 267 pp., 2000.

Flamant, C., Lavaysse, C., Todd, M. C., Chaboureau, J.-P., and Pelon, J.: Multi-platform observations of a springtime case of Bodélé and Sudan dust emission, transport and scavenging over West Africa, Q. J. Roy. Meteor. Soc., 135(639), 413–430, 2009a.

Flamant, C., Knippertz, P., Parker, D., Chaboureau, J.-P., Lavaysse, C., Agusti-Panareda, A., and Kergoat, L.: The impact of a mesoscale convective system cold-pool on the northward propagation of the inter-tropical discontinuity over West Africa, Q. J. Roy. Meteorol. Soc., 135, 139–165, 2009b.

Flamant, C., Chaboureau, J.-P., Parker, D. J., Taylor, C. M., Cammas, J.-P., Bock, O., Timouck, F., and Pelon, J.: Airborne observations of the impact of a convective system on the planetary boundary layer thermodynamics and aerosol distribution in the inter-tropical discontinuity region of the west african monsoon, Q. J. Roy. Meteor. Soc., 133, 1175–1189, doi:10.1002/qj.97, 2007.

Formenti, P., Grand, N., Chevaillier, S., Schmechtig, C., and Desboeufs, K.: Airborne observations of aerosol particles over western Africa in the summer Monsoon season: spatial and vertical variability of physico-chemical and optical properties, Atmos. Chem. Phys. Discuss., in preparation, 2010.

Garcia-Carreras, L., Parker, D. J., Taylor, C. M., Reeves, C. E., and Murphy, J. G.: Impact of mesoscale vegetation heterogeneities on the dynamical and thermodynamic properties of the planetary boundary layer, J. Geophys. Res., 115, D03102, doi:10.1029/2009JD012811, 2010.

Ginoux, P., Chin, M., Tegen, I., Prospero, J. M., Holben, B. N., Dubovik, O., and Lin, S.-L.: Sources and distribution of dust aerosols with the GOCART model, J. Geophys. Res., 106(D17), 20255–20273, 2001.

Gobbi, G. P., Barnaba, F., Van Dingenen, R., Putaud, J. P., Mircea, M., and Facchini, M. C.: Lidar and in situ observations of continental and Saharan aerosol: closure analysis of particles optical and physical properties, Atmos. Chem. Phys., 3, 2161–2172, 2003, http://www.atmos-chem-phys.net/3/2161/2003/.

Goudie, A. S. and Middleton, N. J.: Saharan dust storms: nature and consequences, Earth-Sci. Rev., 56(1), 179–204(26), 2001.

Grini, A., Tulet, P., and Gomes, L.: Dusty weather forecast using the mesonh atmospheric model, J. Geophys. Res., 111, D19205, doi:10.1029/2005JD007007, 2006.

Guerzoni, S., Molinaroli, E., and Chester, R.: Saharan dust inputs to the western Mediterranean Sea: depositional patterns, geochemistry and sedimentological implications, Deep-Sea Res. Pt.II, 44(3–4), 631–654, 1997.

Hopkins, J. R., Evans, M. J., Lee, J. D., Lewis, A. C., H Marsham, J., McQuaid, J. B., Parker, D. J., Stewart, D. J., Reeves, C. E., and Purvis, R. M.: Direct estimates of emissions from the megacity of Lagos, Atmos. Chem. Phys., 9, 8471–8477, 2009, http://www.atmos-chem-phys.net/9/8471/2009/.

Houghton, J. T., Ding, Y., Griggs, D. J., Noguer, M., Van der Linden, P. J., and Xiaosu, D. (Eds.): Climate Change 2001: The Scientific Basis: Contributions of Working Group I to the Third Assessment Report of the Intergovernmental Panel on Climate Change, Cambridge University Press, 881 pp., 2001.

IPCC 2007: Climate Change 2007: The Physical Science Basis. Contribution of Working Group I to the Fourth Assessment Report of the Intergovernmental Panel on Climate Change, edited by: Solomon, S., Qin, D., Manning, M., Chen, Z., Marquis, M., Averyt, K. B., Tignor, M., and Miller, H. L., Cambridge University Press, Cambridge, United Kingdom and New York, NY, USA.

Karyampudi, V. M., Palm, S. P., Reagen, J. A., Fang, H., Grant, W. B., Hoff, R. M., Moulin, C., Pierce, H. F., Torres, O., Browell, E. V., and Melfi, S. H.: Validation of the Saharan dust plume conceptual model using lidar, Meteosat, and ECMWF data, B. Am. Meteorol. Soc., 80, 1045–1075, 1999.

Lafore, J. P., Stein, J., Asencio, N., Bougeault, P., Ducrocq, V., Duron, J., Fischer, C., Hreil, P., Mascart, P., Masson, V., Pinty, J. P., Redelsperger, J. L., Richard, E., and Vilà-Guerau de Arellano, J.: The Meso-NH Atmospheric Simulation System. Part I: adiabatic formulation and control simulations, Ann. Geophys., 16, 90–109, 1998, http://www.ann-geophys.net/16/90/1998/.

Lamb, P. J.: West African water vapor variations between recent contrasting Subsaharan rainy seasons, Tellus, 35A, 198–212, 1983.

Lebel, T., Parker, D. J., Flamant, C., Bourles, B., Marticorena, B., Mougin, E., Peugeot, C., Diedhiou, A., Haywood, J. M., Ngamini, J. B., Polcher, J., Redelsperger, J.-L., and Thorncroft, C. D: The AMMA field campaigns: multiscale and multidisciplinary observations in the West African region, Q. J. R. Meteorol. Soc., in press, doi:10.1002/qj.486, 2010,

Levin, Z., Joseph, J. H., and Mekler, Y.: Properties of Sharav (Khamsin) dust – comparison of optical and direct sampling data, J. Atmosph. Sci., 37, 882–891, 1980.

Levin, Z., Ganor, E., and Gladstein, V.: The effects of desert particles coated with sulfate on rain formation in the eastern Mediterranean, J. Appl. Meteor., 35, 1511–1523, 1996.
Luo, C., Mahowald, N., and del Corral, J.: Sensitivity study of meteorological parameters on mineral aerosol mobilization, transport, and distribution, J. Geophys. Res., 108, 4447, doi:10.1029/2003JD003483, 2003.
Marticorena, B. and Bergametti, G.: Modeling of the atmospheric dust cycle: 1. design of a soil derived dust emission scheme, J. Geophys. Res., 100, 16415–16429, 1995.
Masson, V., Champeaux, J. L., Chauvin, F., Meriguet, C., and Lacaze, R.: A global database of land surface parameters at 1-km resolution in meteorological and climate models, J. Climate, 16(9), 1261–1282, 2003.
Masson, V.: A physically-based scheme for the urban energy balance in atmospheric models, Bound.-Lay. Meteorol., 94, 357–397, 2000.
Mathon, V. and Laurent, H.: Mesoscale convective system rainfall in the Sahel, J. Appl. Meteorol., 41, 1081–1092, 2002.
Middleton, N. J. and Goudie, A. S.: Saharan dust: sources and trajectories, Trans. Inst. Br. Geogr., 26, 165–181, 2001.
Miller, M. A. and Slingo, A.: The ARM Mobile Facility and its first international deployment: Measuring radiative flux divergence in West Africa, Bull. Am. Meteorol. Soc., 88, 1229–1244, 2007.
Noilhan, J. and Mahouf, J.: The isba land surface parametrisation scheme, Global Planet. Change, 13, 145–159, 1996.
Parker D. J., Thorncroft, C. D., Burton, R. R., and Diongue-Niang, A.: Analysis of the African easterly jet, using aircraft observations from the JET2000 experiment, Q. J. Roy. Meteorol. Soc., 131, 1461–1482, 2005a.
Parker, D. J., Burton, R. R., Diongue-Niang, A., Ellis, R. J., Felton, M., Taylor, C. M., Thorncroft, C. D., Bessemoulin, R., and Tompkins, A. M.: The diurnal cycle of the west African monsoon circulation, Q. J. Roy. Meteorol. Soc., 131, 2839–2860, 2005b.
Pinty, J. P. and Jabouille, P.: A mixed-phase cloud parameterization for use in mesoscale non hydrostatic model: simulations of a squall line and of orographic precipitations, Conference of Cloud Physics, Everett, WA, USA, 217–220, 1998.
Prodi, F. and Fea, G.: A case of transport and deposition of Sahara dust over the Italian Peninsula and Southern Europe, J. Geophys. Res., 84C, 6951–6960, 1979.

Prospero, J. M.: Long-term measurements of the transport of African mineral dust to the southeastern United States: Implications for regional air quality, J. Geophys. Res., 104, 15917–15927, 1999.

Redelsperger, J. L., Diedhiou, A., Flamant, C., Janicot, S., Lafore, J. P., Lebel, T., Polcher, J., Bourles, B., Caniaux, G., De Rosnay, P., Desbois, M., Eymard, L., Fontaine, B., Geneau, I., Ginoux, K., Hoepffner, M., Kane, C., Law, K., Mari, C., Marticorena, B., Mougin, E., Pelon, J., Peugeot, C., Protat, A., Roux, F., Sultan, B., and van den Akker, E.: AMMA, une étude multidisciplinaire de la mousson ouest africaine, La Météorologie, aout 2006, vol. 54, 2006.

Reeves, C. E., Formenti, P., Afif, C., Ancellet, G., Attie, J.-L., Bechara, J., Borbon, A., Cairo, F., Coe, H., Crumeyrolle, S., Fierli, F., Flamant, C., Gomes, L., Hamburger, T., Lambert, C., Law, K. S., Mari, C., Matsuki, A., Methven, J., Mills, G. P., Minikin, A., Murphy, J. G., Nielsen, J. K., Oram, D. E., Parker, D. J., Richter, A., Schlager, H., Schwarzenboeck, A., and Thouret, V.: Chemical and aerosol characterisation of the troposphere over West Africa during the monsoon period as part of AMMA, Atmos. Chem. Phys. Disc., in review, 2010.

Sandu, I., Brenguier, J. L., Geoffroy, O., Thouron, O., and Masson, V.: Aerosol impacts on the diurnal cycle of marine stratocumulus, J. Atmos. Sci., 65, 2705–2718, 2008.

Suhre, K., Mari, C., Bates, T. S., Johnson, J. E., Rosset, R., Wang, Q., Bandy, A. R., Blake, D. R., Businger, S., Eisels, F. K., Huebert, B. J., Kok, G. L., Mauldin III, R. L., Prévôt, A. S. H., Schillawski, R. D., Tanner, D. J., and Thornton, T. C.: Physicochemical modeling of the first aerosol characterization experiment (ace 1) lagrangian b, 1. a moving column approach, J. Geophys. Res., 103, 16433–16455, 1998.

Talbot, R. W., Harriss, C., Browell, E. V., Gregory, G. L., Sebacher, D. I., and Beck, S. M.: Distribution and geochemistry of aerosols in the tropical North Atlantic troposphere: Relation to Saharan dust, J. Geophys. Res., 91, 5173–5182, 1986.

Taylor, C. M., Ellis, R. J., Parker, D. J., Burton, R. R., and Thorncroft, C. D.: Linking boundary-layer variability with convection: A case-study from JET2000, Q. J. R. Meteorol. Soc., 129, 2233–2254. doi:10.1256/qj.02.134. 2003.

Taylor, C. M., Parker, D. J., and Harris, P. P.: An observational case study of mesoscale atmospheric circulations induced by soil moisture, Geophys. Res. Lett., 34, L15801, doi:10.1029/2007GL030572, 2007.

Todd, M. C., Bou Karam, D., Cavazos, C., Bouet, C., Heinold, B., Baldasano, J. M., Cautenet, G., Koren, I., Perez, C., Solmon, F., Tegen, I., Tulet, P., Washington, R., and Zakey, A.: Quantifying uncertainty in estimates of mineral dust flux: An intercomparison of model performance over the Bodélé Depression, northern Chad, J. Geophys. Res., 113, D24107, doi:10.1029/2008JD010476, 2008a.

Todd, M. C., Washington, R., Lizcano, G., Ragvahan, S., and Knippertz, P.: Regional model simulations of the Bodélé low-level jet of Northern Chad during BoDEx 2005, J. Clim., 21, 995–1012, 2008b.

Tulet, P., Mallet, M., Pont, V., Pelon, J., and Boon, A.: The 7–13 March 2006 dust storm over West Africa: Generation, transport, and vertical stratification, J. Geophys. Res., 113, D00C08, doi:10.1029/2008JD009871, 2008.

Tulet, P., Crassier, V., Cousin, F., Shure, K., and Rosset, R.: Orilam, a three moment lognormal aerosol scheme for mesoscale atmospheric model, on-line coupling into the mesonh-c model and validation on the escompte campaign, J. Geophys. Res., 110, D18201, doi:10.1029/2004JD005716, 2005.

Tulet, P., Crassier, V., Solmon, F., Guedalia, D., and Rosset, R.: Description of the mesoscale nonhydrostatic chemistry model and application to a transboundary pollution episode between northern france and southern england, J. Geophys. Res., 108(D1), 4021, doi:10.1029/2000JD000301, 2003.

Twomey, S.: The influence of pollution on the shortwave albedo of clouds. J. Atmos. Sci., 34, 1149–1152, 1977.

Warren, A., Chappell, A., Todd, M. C., Bristow, C., Drake, N., Engelstaedter, S., Martins, V., M'Bainayel, S., and Washington, R.: Dust-raising in the dustiest place on Earth, Geomorphology, 92, 25–37, doi:10.1016/j.geomorph.2007.02.007, 2007.

Washington, R. and Todd, M. C.: Atmospheric controls on mineral dust emission from the Bodélé Depression, Chad: The role of the low-level jet, Geophys. Res. Lett., 32, L17701, doi:10.1029/2005GL023597, 2005.

Washington, R., Todd, M. C., Engelstaedter, S., Mbainayel, S., and Mitchell, F.: Dust and the low-level circulation over the Bodele Depression, Chad: Observations from BoDEx 2005, J. Geophys. Res., 111, D03201, doi:10.1029/2005JD006502, 2006.

Zender C. S., Bian, H., and Newman, D.: The mineral dust entrainment and deposition (DEAD) model: Description and global dust distribution, J. Geophys. Res., dust.ess.uci.edu/dead/, 108(D14), 4416, doi:10.1029/2002JD002775, 2003.

Table 1. Log-normal parameters of the size distribution used in the MesoNH model.

Dust mode	fine	medium	coarse
Number (%)	97.52	1.95	0.52
Mass fraction (%)	0.08	0.92	99
Geometric Standard deviation	1.75	1.76	1.70
Number median diameter (µm)	0.078	0.64	5.0
Mass median diameter (µm)	0.20	1.67	11.6

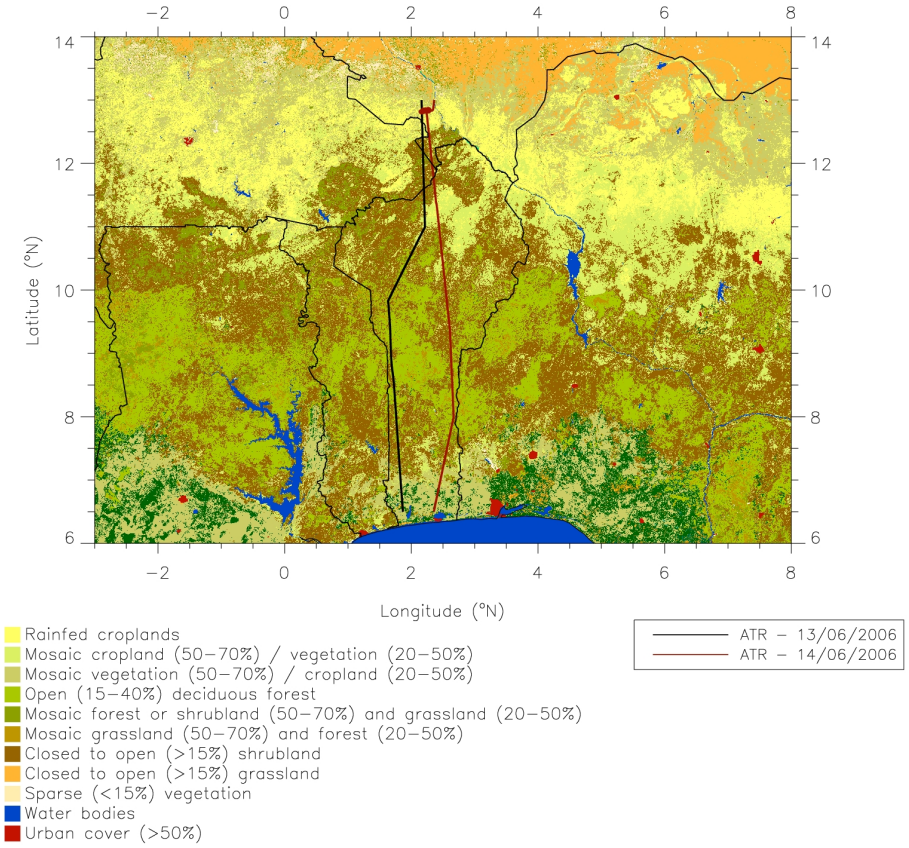

Fig. 1. GlobCover Land Cover map, with the flight plans of the ATR-42 on 13 and 14 June 2006. The map is derived from a time series of MERIS FR mosaics using the UN land Cover Classification System (Source data: ESA/ ESA Globcover project, led by MEDIAS-France/ POSTEL).

ACPD
10, 5051–5090, 2010

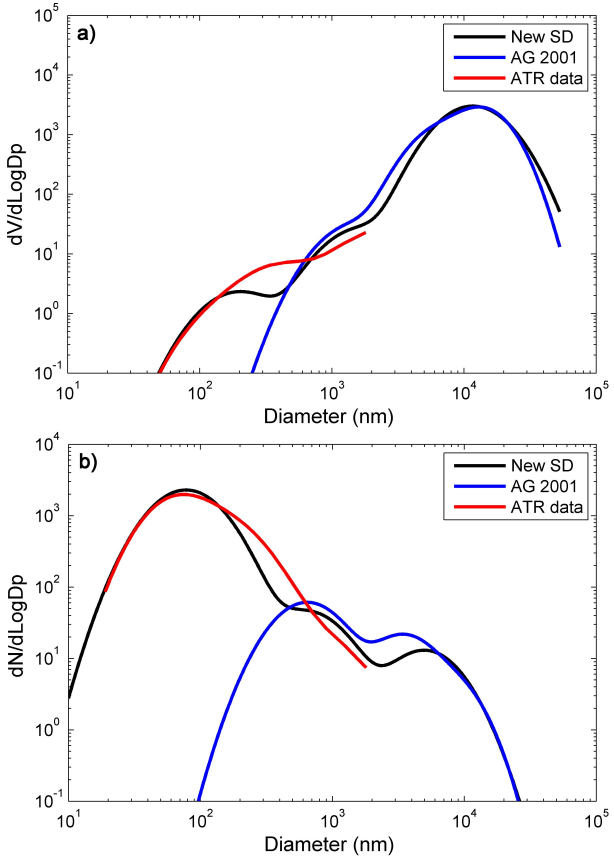

Fig. 2. Volume **(a)** and Number **(b)** size distribution of particles given by Alfaro and Gomes (2001) (blue line), by ATR-42 observations (red line) and the new size distribution (black line) proposed in this study and used in the Meso-NH parametrisation.

ACPD
10, 5051–5090, 2010

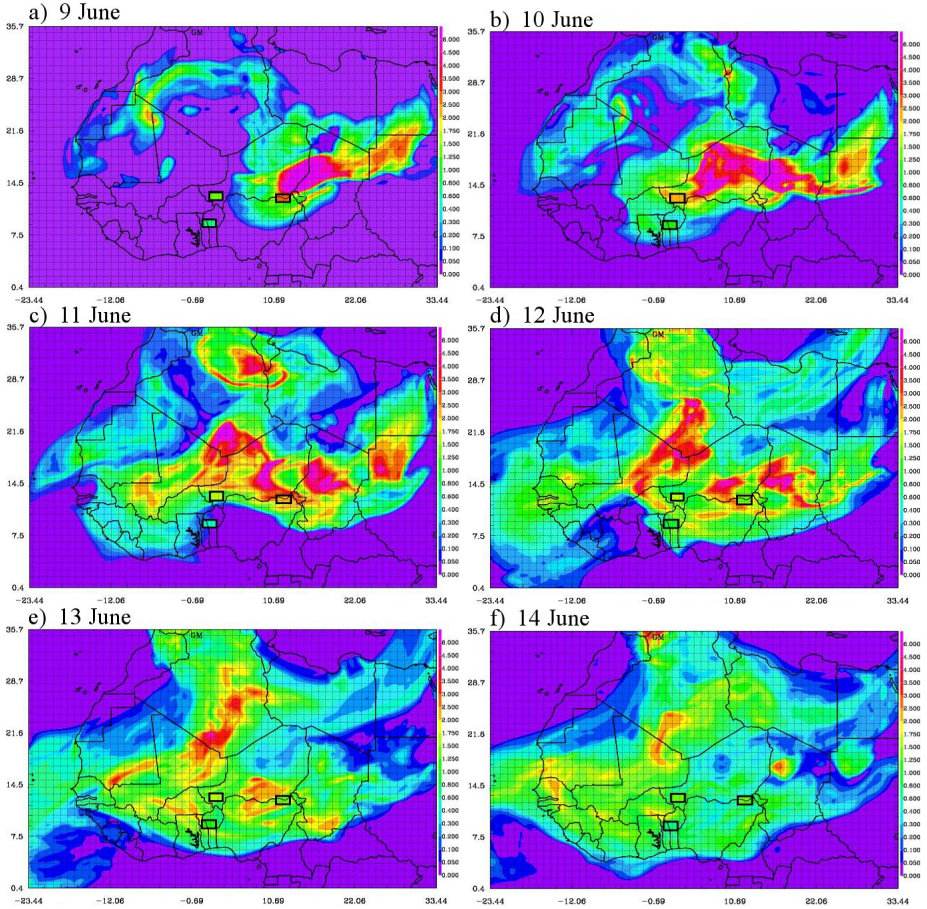

Fig. 3. Daily Aerosol Optical Depth over West Africa from 9 to 14 June 2006, around 12:00 UTC. The simulated AOD values are represented on the whole domain while the observed AOD are represented in boxes.

ACPD
10, 5051–5090, 2010

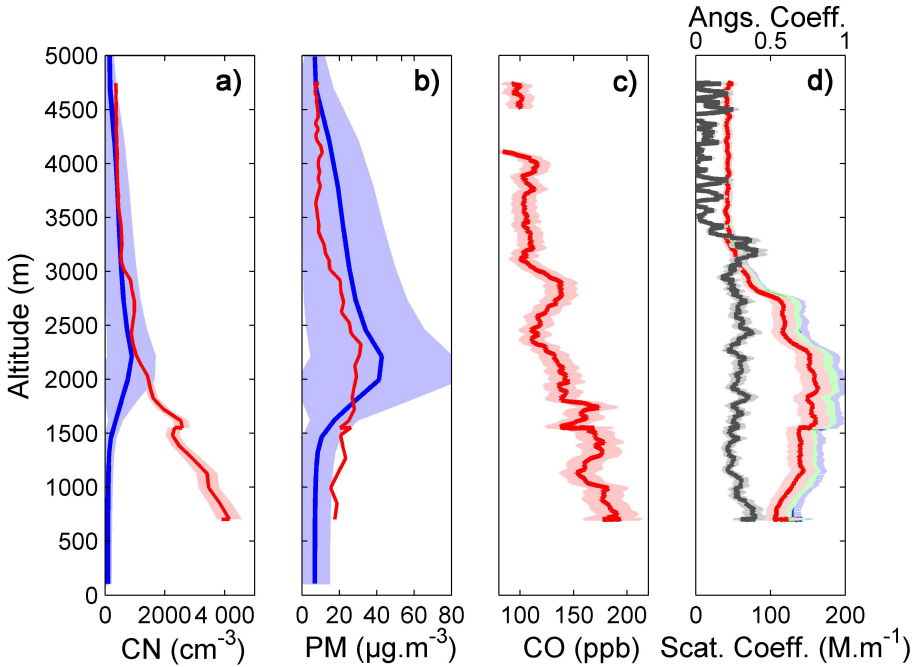

Fig. 4. Profile of the particle number **(a)** and mass **(b)** concentration observed by the ATR-42 at 12.6° N and 2° E between 15:15 UTC and 15:30 UTC on 14 June 2006 (red lines). The simulated number (a) and mass (b) concentration of particles (15:00 UTC on 14 June 2006), at 12.6° N and 2° E (blue lines). The blue areas correspond to the spatial variability (1° around the ATR-42 sounding zone) of dust concentration for particles with diameter lower then 2.5 µm. Profiles of the CO concentration **(c)** and the scattering coefficient for three wavelengths (450 nm, 550 nm, 700 nm; respectively blue, green and red lines) **(d)** observed by the ATR-42 are also plotted. On (d), the black line represents the calculated Angstrom coefficient and the coloured areas correspond to the instrumentfs internal variability.

ACPD
10, 5051–5090, 2010

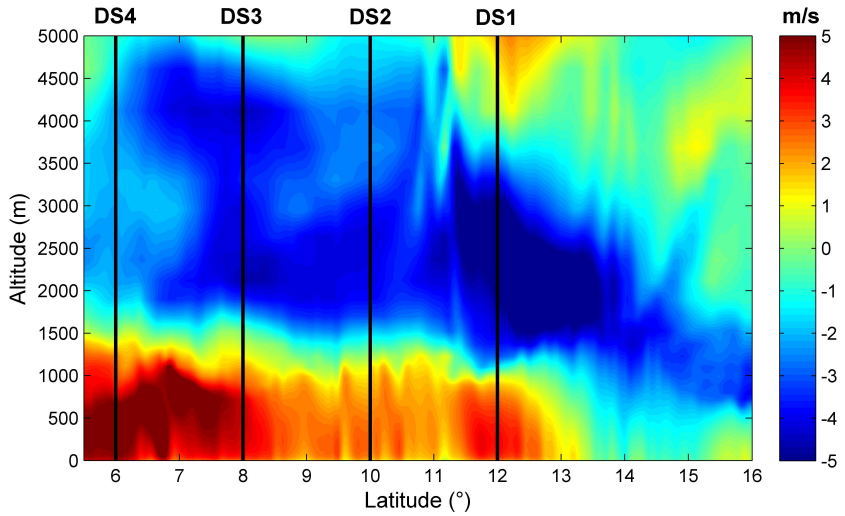

Fig. 5. Vertical cross section (along the ATR-42 flight track 2.00° E) of the meridional component of the simulated wind ($m\,s^{-1}$). The black lines indicate the location of the dropsondes released by the F-F20 along the transect. The numbers refer to the dropsonde numbers as they appear in Fig. 6.

ACPD
10, 5051–5090, 2010

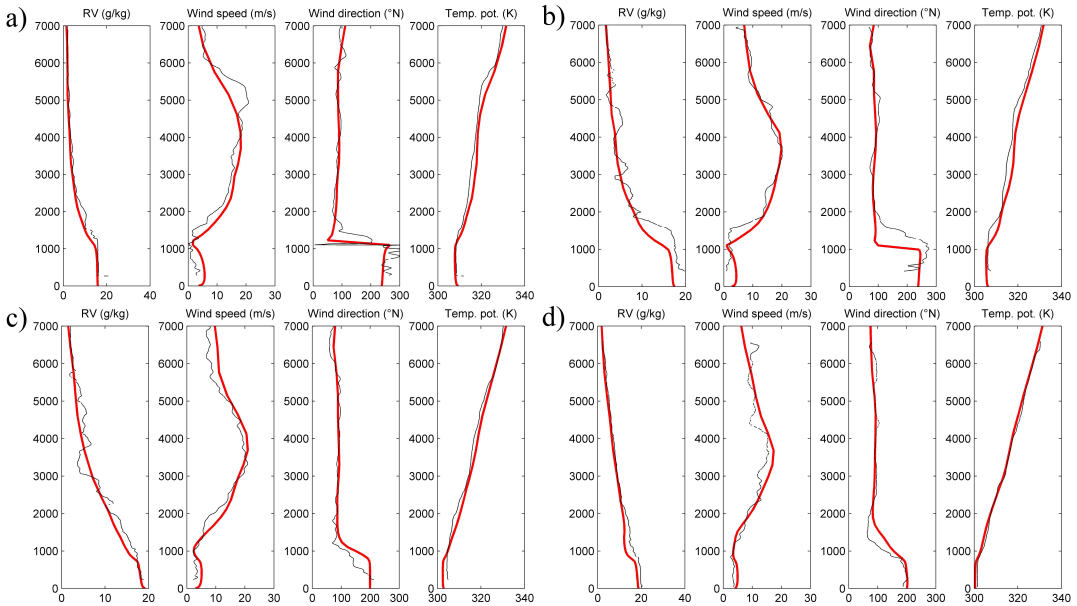

Fig. 6. Vapour mixing ratio ($g\,kg^{-1}$), wind speed ($m\,s^{-1}$) wind direction (°N) and potential temperature (K) derived from dropsonde measurements (red lines) and the MESONH simulation (black lines) at 12° N (a, DS1), at 10° N (b, DS2), at 8°N (c, DS3) and at 6°N (d, DS4) on 13 June.

ACPD
10, 5051–5090, 2010

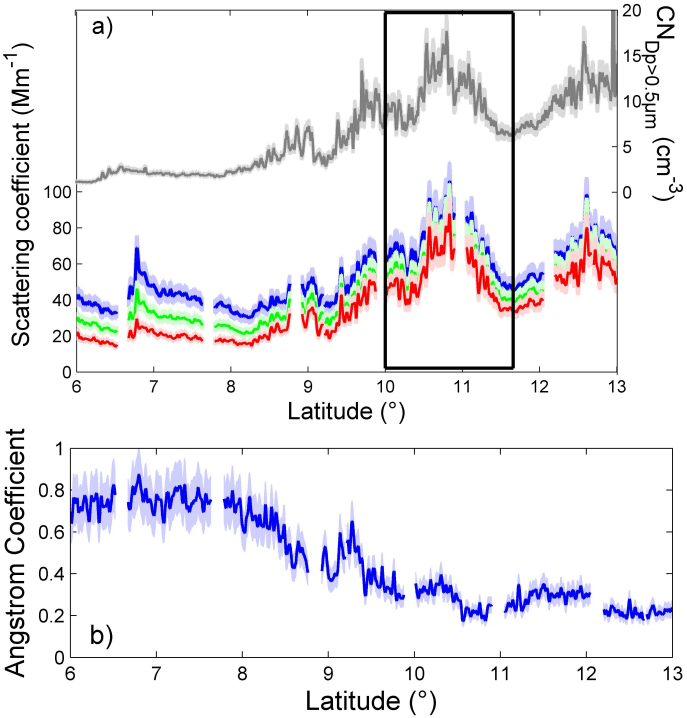

Fig. 7. **(a)** Scattering coefficient observed on-board the ATR-42 between 10:30 UTC and 13:30 UTC on 13 June for 3 different wavelengths are represented using blue (450 nm), green (550 nm) and red (700 nm) lines as a function of latitude. Concentration of particles with diameter higher than 0.5 µm is plotted in grey as a function of latitude. The black rectangle denotes the zone where the dust content is maximum. **(b)** The Angstrom coefficient calculated from scattering coefficients is represented by the blue line. The light blue area corresponds to the error bar including uncertainty in the measurements of scattering coefficients and propagation of errors during calculations.

ACPD
10, 5051–5090, 2010

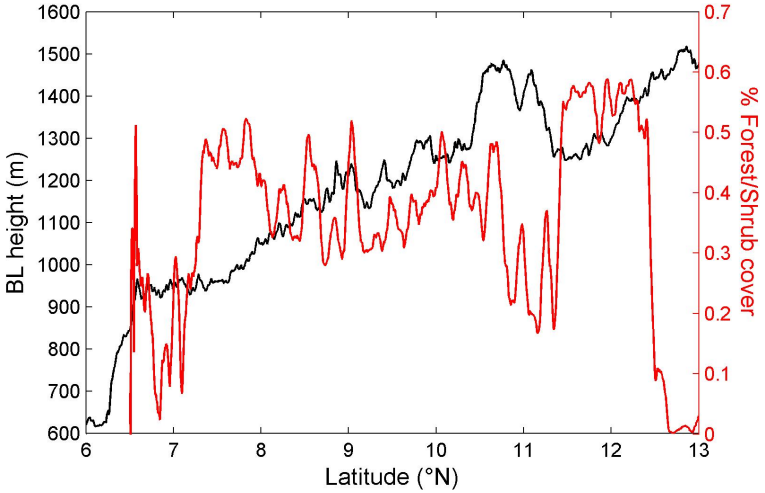

Fig. 8. Calculated boundary layer top (black line) and fraction of forest/shrub cover as derived from the GlobCover Land Cover map (red line) as a function of latitude.

ACPD
10, 5051–5090, 2010

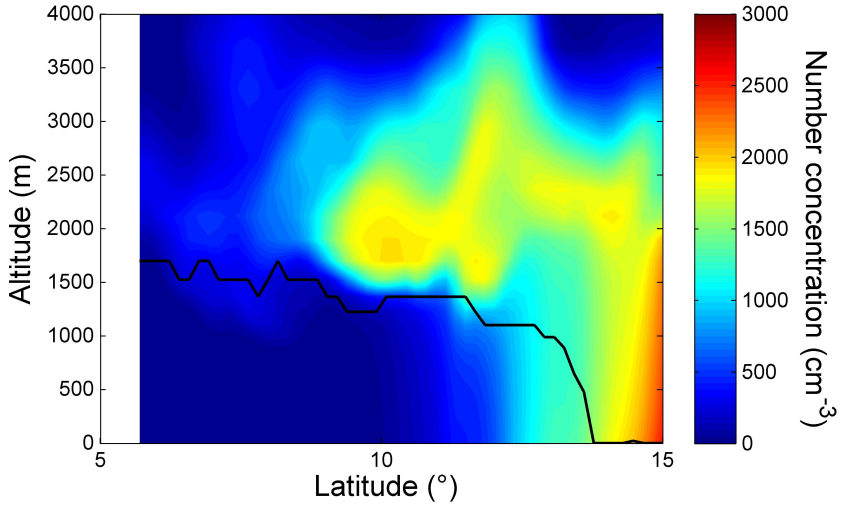

Fig. 9. Cross-section of dust number concentration for the simulation including sedimentation (NORAD-SED). The black line illustrates the top of the monsoon flux.

ACPD
10, 5051–5090, 2010

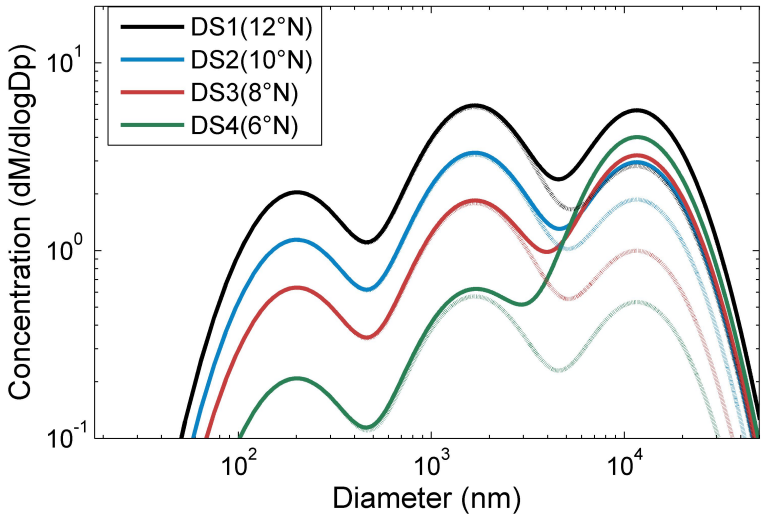

Fig. 10. Mass size distribution for the SED simulation (line) and the NOSED simulation (dashed line) of dust particles tranported in the Saharan Air Layer (SAL), at 2000 m, for different latitudes (12° N, 10° N, 8° N, 6° N).

ACPD
10, 5051–5090, 2010

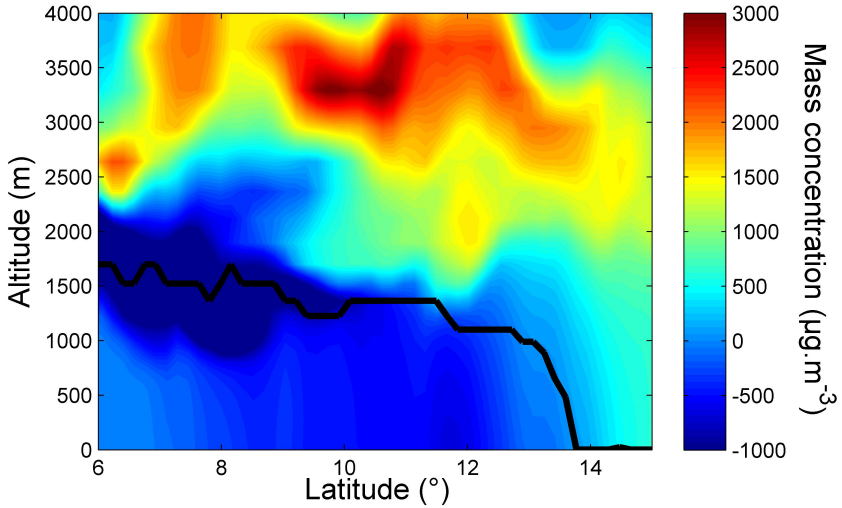

Fig. 11. Difference of dust mass concentration between the simulation without sedimentation (NOSED) and the simulation including sedimentation (SED; see text for more details). Negative mass concentrations correspond to sedimented particles. The black line illustrates the top of the monsoon flux.

ACPD
10, 5051–5090, 2010

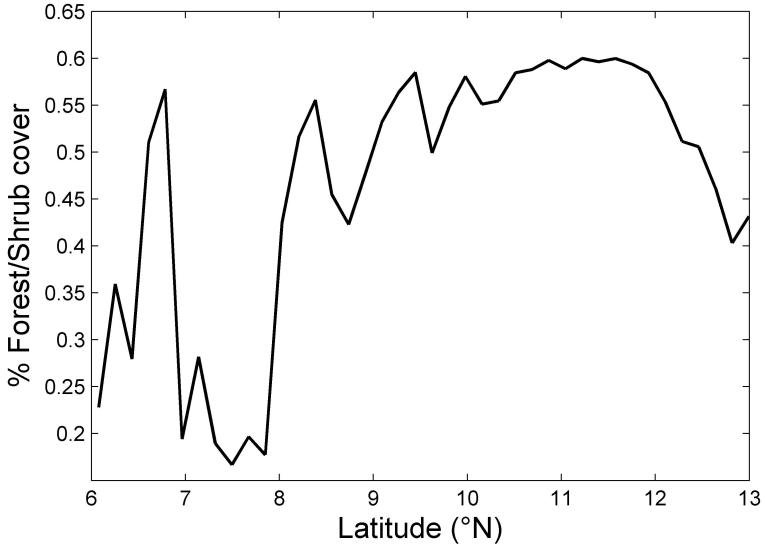

Fig. 12. Fraction of forest/shrub cover taken into account in Meso-NH (black line).

ACPD
10, 5051–5090, 2010